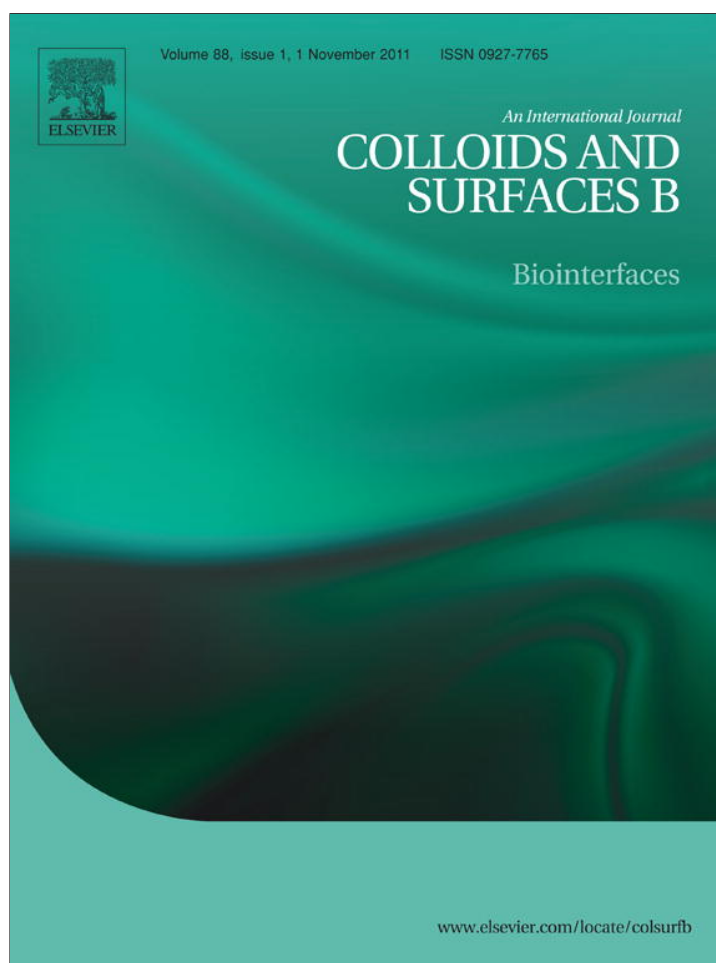


Provided for non-commercial research and education use.
Not for reproduction, distribution or commercial use.



This article appeared in a journal published by Elsevier. The attached copy is furnished to the author for internal non-commercial research and education use, including for instruction at the authors institution and sharing with colleagues.

Other uses, including reproduction and distribution, or selling or licensing copies, or posting to personal, institutional or third party websites are prohibited.

In most cases authors are permitted to post their version of the article (e.g. in Word or Tex form) to their personal website or institutional repository. Authors requiring further information regarding Elsevier's archiving and manuscript policies are encouraged to visit:

<http://www.elsevier.com/copyright>



Contents lists available at ScienceDirect

Colloids and Surfaces B: Biointerfaces

journal homepage: www.elsevier.com/locate/colsurfb

Structural and dynamical characterization of unilamellar AOT vesicles in aqueous solutions and their efficacy as potential drug delivery vehicle

Ranajay Saha, Pramod Kumar Verma, Rajib Kumar Mitra*, Samir Kumar Pal*,¹

Unit for Nano Science & Technology, Department of Chemical, Biological & Macromolecular Sciences, S.N. Bose National Centre for Basic Sciences, Block JD, Sector III, Salt Lake, Kolkata 700098, India

ARTICLE INFO

Article history:

Received 15 March 2011
 Received in revised form 17 June 2011
 Accepted 5 July 2011
 Available online 12 July 2011

Keywords:

Unilamellar AOT vesicles
 Dynamic light scattering
 Förster resonance energy transfer (FRET)
 Arrhenius energy
 Picosecond resolved temperature dependent dynamics
 Controlled drug release

ABSTRACT

Sodium bis(2-ethylhexyl) sulfosuccinate (AOT) is well known to form nanometre sized aqueous droplets in organic solvents and used in several contemporary applications including templates of nanoparticle synthesis. However, the detailed structural characterization of AOT in aqueous media is relatively less attended. Here we have used dynamic light scattering technique for the structural characterization of AOT in aqueous solutions and found to have a monodispersed, unilamellar vesicles (~140 nm diameter). The efficacy of the vesicle to host both charged drugs like H258 (2'-(4-hydroxyphenyl)-5-[5-(4-methylpiperazine-1-yl)-benzimidazo-2-yl-benzimidazole]), EtBr (ethidium bromide) and hydrophobic drug like DCM (4-(dicyanomethylene)-2-methyl-6-(p-dimethylamino-styryl)-4H-pyran) has also been investigated using Förster resonance energy transfer. Picosecond resolved and polarization gated spectroscopy have been used to study the solvation dynamics and microviscosity at the surface of the vesicles. We have also performed concentration and temperature dependent studies in order to confirm the stability of the vesicles in aqueous phase. The drug release profile of the vesicles has been studied through in vitro dialysis method. The non-toxic, monodispersed vesicles in aqueous media with a noteworthy stability in wide range of AOT concentration and temperature, capable of hosting drugs of various natures (both hydrophobic and charged) simultaneously for many codelivery applications with controlled drug release profile may find its applications in drug delivery.

© 2011 Elsevier B.V. All rights reserved.

1. Introduction

Unilamellar vesicles (ULV) have considerable structural similarity with biological membranes including high encapsulation property, permeability and have widely been used in several applications including biomimicking [1], drug delivery [2], synthesis of nanoparticles [3], biochemical catalysis [4], cosmetics [4], etc. The water pool of ULVs encapsulates aqueous soluble drugs within its central aqueous compartment as well as hydrophobic drugs within the bilayer membrane that forms the wall. Vesicles have caught much attention as drug carriers because they can offer the advantage of improving the therapeutic activity of drugs, reducing drug toxicities, and decreasing the drug dosage [5]. They also behave as well recognised controlled release systems (CRS) [6,7] that can maintain drug concentration in the blood or in targeted tissues at a desired value for a considerable period of time [8,9] rendering

a control on the drug release rate and duration [10]. For this purpose, in general, CRS initially releases the dose contained in parts so as to rapidly achieve at the drug effective therapeutic concentration. Such drug release kinetics follows a well defined behaviour in order to supply the maintenance dose enabling the attainment of the desired drug concentration.

Preparation of vesicles involves rather simple and straightforward approach. In one of the methods it is formed by phospholipids that usually require some additional energy like ultrasonication [11]. The vesicles thus obtained are metastable and easy to fuse. On the other hand, the spontaneous formation of thermodynamically stable, long lived vesicles has been realized in a variety of aqueous surfactant solutions [12–24]. Out of these Aerosol OT (sodium bis(2-ethylhexyl) sulfosuccinate, AOT) is a well-studied surfactant, which forms reverse micelles (RMs) of well-defined structure in organic oil [25]. It is a versatile double tailed medicinal surfactant [26] which is known as a transdermal drug delivery vehicle in normal micellar form [27]. By virtue of its nontoxicity, spontaneously formed and thermodynamically stable long lived AOT vesicles in unilamellar form might establish a potential application. Phase diagram of AOT/water mixtures obtained using small-angle neutron scattering technique [28] and X-ray experiments [29] reveal a considerably large lamellar liquid crystalline phase D (10–70 wt%

* Corresponding authors. Tel.: +91 033 2335 5706–08; fax: +91 033 2335 3477.

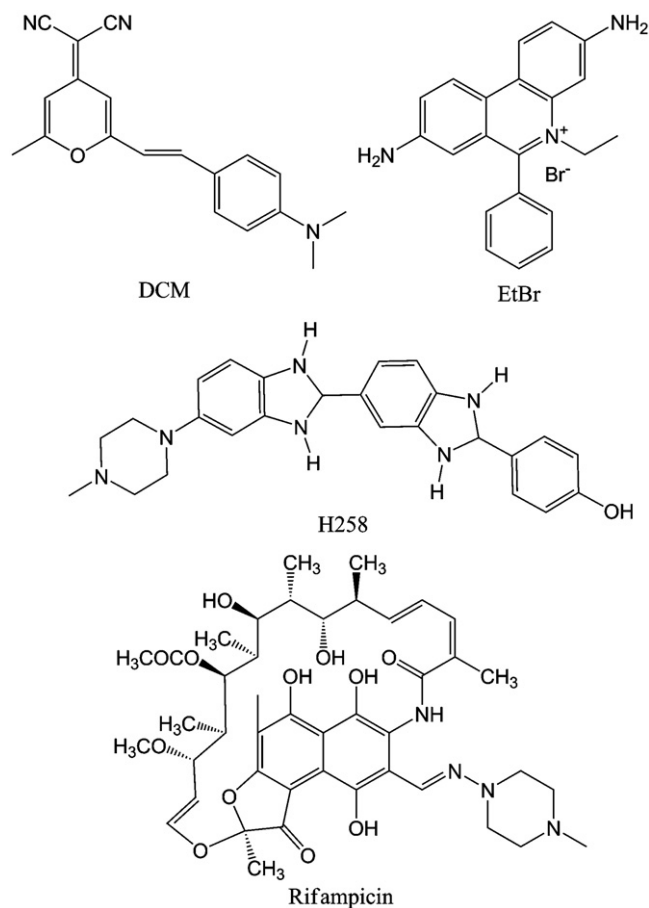
E-mail addresses: rajib@bose.res.in (R.K. Mitra), skpal@bose.res.in (S.K. Pal).¹ Present address: Arthur Amos Noyes Laboratory of Chemical Physics, California Institute of Technology (CALTECH), 1200 East California Boulevard, Pasadena, CA 91125, USA.

surfactants) in the phase map. A bicontinuous-type cubic phase (73–80 wt% AOT) and a reverse hexagonal liquid crystalline phase (>82 wt% AOT) are also formed in the surfactant-rich region of the phase diagram. The water-rich side in the phase map is largely biphasic with the D phase in equilibrium with a solution phase, and below 1.3 wt%, the surfactant is soluble in water. Although the detailed phase diagram of AOT-water system is available in literature, a comprehensive understanding of the structure and dynamics of the vesicle-forming water-rich region needs to be extensively studied as only a handful of reports are available in the literature that relate various morphologies and mechanical properties of AOT vesicle [30,31]. Moreover, complete characterization of the aggregate structure in aqueous solution (unilamellar or multilamellar) including dynamical states of water in such systems at different temperatures have not yet been attempted and is one of the motives of our present study. Meanwhile, in the light of wide versatility (e.g. application in the contraception, ophthalmic and odontoiatric fields, in the treatment of cancer, alcoholism, diabetes, thrombosis [32]), controlled release profile is an obvious characteristics of drug delivery vehicles for the exploitation of the modern concept of therapeutic treatment which aims to increase drug effectiveness and patient compliance, to reduce the administration frequency and side effects connected to dosing. With this background study of drug release profile of AOT vesicles and its associated kinetics are complementary interests of our present study.

In this study we demonstrate that the combination of spectroscopic and light scattering methods is a powerful approach to reveal aggregate structure and size of AOT vesicles in dilute region. Structural integrity of the vesicle has been studied over a range of concentration (9–18 mM) and temperature (293–343 K) using dynamic light scattering (DLS) technique. The aging stability of the structure has also been confirmed using DLS. The efficacy of the vesicles to host small model drugs/ligands viz. 2'-(4-hydroxyphenyl)-5-[5-(4-methylpiperazine-1-yl)-benzimidazo-2-yl]-benzimidazole (H258), ethidium bromide (EtBr) and 4-(dicyanomethylene)-2-methyl-6-(p-dimethylamino-styryl)-4H-pyran (DCM) has been investigated using picosecond-resolved fluorescence spectroscopy. The dye DCM is hydrophobic in nature and is well known for its ability to report the interfacial water relaxation dynamics in micelles [33], RMs [34] and liposomes [35]. The solvatochromic property of DCM has been used to study the dynamics of solvation and also to eliminate the possible existence of multilamellar AOT/water vesicles in the studied systems. Polarization gated anisotropy of DCM has been studied in order to determine the microviscosity at the surface of AOT/water vesicle. Förster resonance energy transfer (FRET) between the dyes H258 (donor)-DCM (acceptor) and H258 (donor)-EtBr (acceptor) in the studied AOT vesicle system have been successfully used to investigate the ability of the vesicles to host both hydrophobic and charged drugs simultaneously. In vitro drug release studies show a controlled release profile of the model drug rifampicin from AOT vesicle with its pH sensitivity in release. We attempt to establish AOT/water vesicle as a safe and promising drug delivery vehicle.

2. Materials and methods

Chemicals were obtained from the following sources: sodium bis(2-ethylhexyl) sulfosuccinate (AOT, Sigma); 4-(dicyanomethylene)-2-methyl-6-(p-dimethylamino-styryl)-4H-pyran (DCM, Fluka); 2'-(4-hydroxyphenyl)-5-[5-(4-methylpiperazine-1-yl)-benzimidazo-2-yl]-benzimidazole (H258, Molecular Probes); ethidium bromide (EtBr, Molecular Probes), rifampicin (Sigma Aldrich) (Scheme 1). Transparent solutions of vesicles were



Scheme 1. Molecular structure of DCM, EtBr, H258 and rifampicin.

prepared by adding calculated amount of surfactant to water followed by gentle stirring. For vesicles containing probe molecules the respective probe was added before stirring the solutions. Prior to all the measurements, the AOT/water solutions were filtered with a Whatman syringe filter (pore size of 0.2 μm). DLS measurements were done with Nano S Malvern-instrument employing a 4 mW He-Ne laser ($\lambda = 632.8 \text{ nm}$) equipped with a thermostated sample chamber. All the scattered photons are collected at 173° scattering angle. The scattering intensity data are processed using the instrumental software to obtain the hydrodynamic diameter (d_H) and the size distribution of the scatterer in each sample. The instrument measures the time dependent fluctuation in the intensity of light scattered from the particles in solution at a fixed scattering angle. Hydrodynamic diameter (d_H) of the vesicle is estimated from the intensity auto-correlation function of the time-dependent fluctuation in intensity. d_H is defined as

$$d_H = \frac{k_B T}{3\pi\eta D} \quad (1)$$

where k_B is the Boltzmann constant, η the viscosity, and D the translational diffusion coefficient. In a typical size distribution graph from the DLS measurement, the x-axis shows a distribution of size classes in nanometres, while the y-axis shows the relative intensity of the scattered light. This is therefore known as an intensity distribution graph. DLS experiments were done in triplicate with at least 15 runs per measurement.

Steady-state emissions were measured with a Jobin Yvon Fluoromax-3 fluorimeter, with a temperature controlled attachment from Julabo (Model: F32). Fluorescence transients were measured by using a commercially available spectrophotometer

(LifeSpec-ps) from Edinburgh Instruments, UK (excitation wavelength of 375 nm (for DCM & H258 in AOT vesicles) and 409 nm (for EtBr in AOT vesicles), 80 ps instrument response function (IRF)). The observed fluorescence decay transients are fitted by using a nonlinear least square fitting procedure [33] to a function ($X(t) = \int_0^t E(t')R(t-t')dt'$) comprising of convolution of the IRF ($E(t)$) with a sum of exponentials ($R(t) = A + \sum_{i=1}^N B_i e^{-t/\tau_i}$) with pre-exponential factors (B_i), characteristic lifetimes (τ_i) and a background (A). Relative concentration in a multi-exponential decay is finally expressed as $a_n = B_n / \sum_{i=1}^N B_i$. The quality of the curve fitting is evaluated by reduced chi-square and residual data.

To construct time-resolved emission spectra (TRES) we follow the technique described in Refs. [33,36]. The time-dependent fluorescence Stokes shifts, as estimated from TRES, are used to construct the normalized spectral shift correlation function or the solvent correlation function, $C(t)$, defined as

$$C(t) = \frac{\nu(t) - \nu(\infty)}{\nu(0) - \nu(\infty)} \quad (2)$$

where $\nu(0)$, $\nu(t)$ and $\nu(\infty)$ are the emission maxima (in cm^{-1}) at time zero, t and infinity, respectively. The $C(t)$ function represents the temporal response of the solvent relaxation process, as occurs around the probe following its photo excitation and the associated change in the dipole moment. For anisotropy ($r(t)$) measurements, emission polarization was adjusted to be parallel or perpendicular to that of the excitation, and anisotropy is defined as [36]:

$$r(t) = \frac{I_{\parallel}(t) - I_{\perp}(t)}{I_{\parallel}(t) + 2I_{\perp}(t)} \quad (3)$$

where $I_{\parallel}(t)$ and $I_{\perp}(t)$ are the temporal emission intensities at parallel and perpendicular emission polarization with respect to vertical excitation polarization.

The rotational time constants were calculated using the reported method for fluorescence anisotropy analysis [37]. In this analysis the basic equations used to fit the parallel ($I_{\parallel}(t)$) and perpendicular ($I_{\perp}(t)$) components of the emission transients are,

$$I_{\parallel}(t) = \frac{1}{3}F(t)[1 + 2r(t)] \quad (4a)$$

$$I_{\perp}(t) = \frac{1}{3}F(t)[1 - r(t)] \quad (4b)$$

where $F(t)$ is the pure excited state population decay, free of anisotropy effect; can be written as $F(t) = F_0 \exp(-t/\tau_F)$; τ_F being the average lifetime of the fluorophore estimated from the reconvolution fitting analysis of fluorescence decay taken at magic angle 54.7° . $r(t)$ is the anisotropy decay at time t and is given by,

$$r(t) = a_{fast} \exp\left(\frac{-t}{\tau_{fast}}\right) + a_{slow} \exp\left(\frac{-t}{\tau_{slow}}\right) \quad (5)$$

where τ_{fast} and τ_{slow} are the rotational time constants and a_{fast} and a_{slow} being their relative weight respectively in the total anisotropy. Substituting $r(t)$ and $F(t)$ into Eq. (4) yields,

$$I_{\parallel}(t) = F_0 \exp(-t/\tau_F) + 2a_{fast}F_0 \exp\left(-\frac{t}{\tau_{fast}\tau_F/(\tau_{fast} + \tau_F)}\right) + 2a_{slow}F_0 \exp\left(-\frac{t}{\tau_{slow}\tau_F/(\tau_{slow} + \tau_F)}\right) \quad (6a)$$

$$I_{\perp}(t) = F_0 \exp(-t/\tau_F) - a_{fast}F_0 \exp\left(-\frac{t}{\tau_{fast}\tau_F/(\tau_{fast} + \tau_F)}\right) - a_{slow}F_0 \exp\left(-\frac{t}{\tau_{slow}\tau_F/(\tau_{slow} + \tau_F)}\right) \quad (6b)$$

Now both $I_{\parallel}(t)$ and $I_{\perp}(t)$ decays can be fitted tri-exponentially as,

$$I_{\parallel}(t) = A_1 \exp\left(\frac{-t}{\tau_a}\right) + A_2 \exp\left(\frac{-t}{\tau_b}\right) + A_3 \exp\left(\frac{-t}{\tau_c}\right) \quad (7a)$$

$$I_{\perp}(t) = A'_1 \exp\left(\frac{-t}{\tau_a}\right) + A'_2 \exp\left(\frac{-t}{\tau_b}\right) + A'_3 \exp\left(\frac{-t}{\tau_c}\right) \quad (7b)$$

where τ_i represents fitted time parameters and A_i its relative weight.

Comparing Eq. (6) with Eq. (7) one can find out the values of τ_{fast} , τ_{slow} , a_{fast} and a_{slow} and the calculated values are reported in Table 2. All the anisotropy results are averaged over three independent measurements.

In order to estimate Förster resonance energy transfer efficiency of the donor (H258) and hence to determine the distance of donor-acceptor pairs we used the following methodology [36]. The Förster distance (R_0) is given by,

$$R_0 = 0.211[\kappa^2 n^{-4} Q_D J(\lambda)]^{1/6} \quad (8)$$

where κ^2 is a factor describing the relative orientation in space of the transition dipoles of the donor and acceptor. For donor and acceptors that are randomized by rotational diffusion prior to energy transfer, the magnitude of κ^2 is assumed to be $2/3$. The refractive index (n) of the medium was calculated to be 1.334 ± 0.001 using Rudolph J357 automatic refractometer. Q_D , the quantum yield of the donor in the absence of acceptor was measured to be 0.36 using the quantum yield of H258 in ethanol as reference standard (Q_D of H258 in ethanol is 0.50 [38]), $J(\lambda)$ the overlap integral, which expresses the degree of spectral overlap between the donor emission and the acceptor absorption is given by,

$$J(\lambda) = \frac{\int_0^\infty F_D(\lambda)\varepsilon_A(\lambda)\lambda^4 d\lambda}{\int_0^\infty F_D(\lambda)d\lambda} \quad (9)$$

where $F_D(\lambda)$ is the fluorescence intensity of the donor in the wavelength range of λ to $(\lambda + d\lambda)$ and is dimensionless. $\varepsilon_A(\lambda)$ is the extinction coefficient (in $\text{M}^{-1} \text{cm}^{-1}$) of the acceptor at λ . If λ is in nm, then $J(\lambda)$ is in units of $\text{M}^{-1} \text{cm}^{-1} \text{nm}^4$. Once the value of R_0 is known, the donor-acceptor distance (r) can be easily calculated using the formula,

$$r^6 = \frac{R_0^6(1-E)}{E} \quad (10)$$

where E is the efficiency of energy transfer. The transfer efficiency (E) is measured using the fluorescence lifetime of the donor, in absence (τ_D) and presence (τ_{DA}) of the acceptor.

$$E = 1 - \frac{\tau_{DA}}{\tau_D} \quad (11)$$

The reported FRET results are averaged for three independent measurements.

In vitro release was determined by the dialysis bag method [39]. To perform the study, 1.5 ml of 18 mM AOT vesicle solution containing 400 μM of rifampicin was taken in a dialysis bag (Spectrum Laboratories, Inc, USA, MWCO:12,000–14,000 Da) and was tightly sealed. The sealed dialysis bag was then introduced into 40 ml of in vitro release medium of either phosphate buffered saline (10 mM, pH 7.4) or citrate buffer solution (10 mM, pH 5.8). The whole system was incubated at 37°C under stirring condition at a constant speed. Aliquots of 2 ml were withdrawn from the release medium at selected time intervals for 24 h and replaced

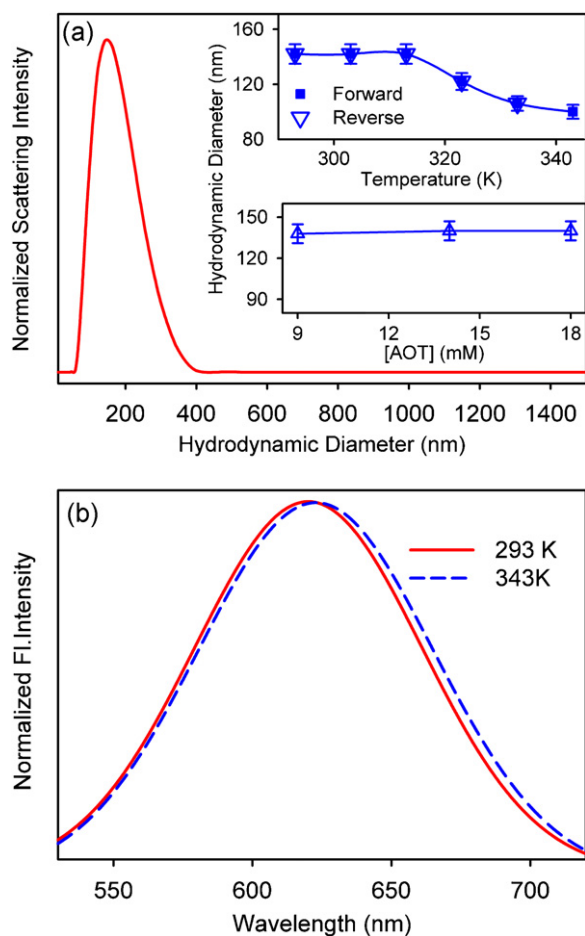


Fig. 1. (a) A typical dynamic light scattering (DLS) signal of 18 mM AOT/water vesicle at 293 K. Change in hydrodynamic diameter of 18 mM AOT/water vesicles at different temperatures in both forward and reverse modes have been shown in the inset. The concentration independent vesicle diameter is shown in another inset. (b). Emission spectrum of DCM excited at 375 nm in 18 mM AOT/water vesicle at 293 K and 343 K.

with equal volume of fresh buffer to keep the release medium volume constant. The released amount of rifampicin in each aliquot was determined from the absorbance at 334 nm and the percentage released in the bulk was calculated as a function of incubation time. Control experiments were done by taking only 400 μ M of rifampicin in the dialysis bag against identical release medium under identical experimental condition. Release experiments were repeated for at least thrice to ensure their reproducibility.

3. Results and discussions

In order to measure the size of the self-aggregates of AOT in dilute aqueous solution, dynamic light scattering (DLS) measurements are carried out at three different AOT concentrations (9, 14 and 18 mM; inset of Fig. 1a) and at various temperatures. A representative intensity distribution curve for 18 mM AOT solution is presented in Fig. 1a which indicates an aggregate size of \sim 140 nm. Similar size distribution is obtained with 9 and 14 mM AOT concentrations. It can be emphasized here that the distribution profile is unimodal in both intensity ($\propto d^6$) distribution as well as in volume ($\propto d^3$) distribution profile (d being the diameter of particles) with relatively low (\sim 0.2) polydispersity index (PDI) suggesting the existence of aggregates of uniform sizes. Here the higher hydrodynamic diameter with unimodal size distribution indicates the formation of AOT vesicles rather than self assembly of AOT molecules to form

micelles. The previously reported CVC (critical vesicle concentration) of 7.8 mM [30,40] and CMC (critical micelle concentration) of 2.66 mM [41–43] strongly suggest the preferential formation of vesicles in the studied concentration range. An important question is worth introducing here is whether the vesicles are unilamellar or multilamellar. It is known that geometrical properties of multilamellar vesicles (MLV) depend upon the concentration of the vesicle forming amphiphile and increase in amphiphile concentration adds up new layers in MLV resulting in a concentration dependent growth of vesicle size [44]. The uniformity in the concentration independent size distribution of vesicles in the present study confirms the ULV formation. Temperature dependent DLS study (inset of Fig. 1a) shows a single monodispersed (with low PDI) peak with a slight decrease in the vesicle size with temperature. Shading of water molecules from hydration layer, as has also been observed in micelles at higher temperature [33] is an obvious reason for this change, moreover, the increased contribution of faster moving bulk water [45] (which extends from fs to ps) at higher temperature also limits the estimation of hydration layer by slow DLS (which extends from ns to ms) technique to a smaller value. It is also to be noted here that self-assembled structures (like micelles, reverse micelles, vesicles, etc.) retain a dynamic equilibrium in solution which manifests dynamic exchange of solutes (amphiphiles), and is a function of temperature and solvent properties. Exclusion of water from the vesicle-pool during the dynamic exchange of solutes at higher temperature might be one of the reasons for this change. Thus the change in the vesicle size is a cumulative approach and its reversibility provides evidence of the very physical nature of the size reduction. The overall retention of size and monodispersity provides evidence of existence of only vesicle structures even at elevated temperatures.

The aging effect on the size of the vesicles is examined by DLS experiment. Freshly prepared vesicles show a diameter of about \sim 140 nm and it remains unchanged even after 15 days with an almost unchanged PDI value (\sim 0.2) (Supporting Information, Table S1). The transparency of the solution is also found to be retained with aging confirming the stability of the ULV with time, which is a prerequisite for a potential drug delivery vehicle.

As the vesicles are non-fluorescent, the spectroscopic study is probed by DCM. Fig. 1b depicts the fluorescence spectra of DCM in 18 mM AOT vesicle, excited at 375 nm, at 293 and 343 K. The emission peak, which is obtained at 620 nm at 293 K, is consistent with the value found for DCM in Triton X-100, cetyl trimethyl ammonium bromide and sodium dodecyl sulfate micelles [46]. The position of the emission maximum of DCM in AOT vesicle is found to be similar to that in highly polar solvents, e.g. methanol, formamide, etc. [47,48]. It may be recalled here that in pure hydrocarbon (e.g. n-heptane) DCM exhibits very weak emission with quantum yield of 0.01 and emission maximum at 530 nm [34]. The emission quantum yield of DCM is also known to increase with increase in solvent polarity and is 0.44 in methanol [49]. The red shifted emission maximum (620 nm) and relatively high quantum yield (0.36) value of DCM in AOT vesicles suggest that DCM molecules stay in the polar interface of the vesicles instead of the dry hydrocarbon layer. The insignificant red shift (\sim 2 nm) (Fig. 1b) in the peak position of the probe at higher temperature signifies that the microenvironment of the probe does not change appreciably with temperature and it resides in the interface only.

To probe the dynamics of water entrapped in the AOT vesicles we study the picosecond-resolved fluorescence spectroscopy of the solvation probe, DCM. The Fluorescence decay transients of DCM in AOT vesicles at three representative wavelengths at 293 K are presented in Fig. 2a. It is evident from the figure that the decay patterns are strongly wavelength dependent. At 560 nm, the transient decays fast with time components of 140 ps (60%), 670 ps (30%) and 1680 ps (10%). For the extreme red wavelength (680 nm), a distinct

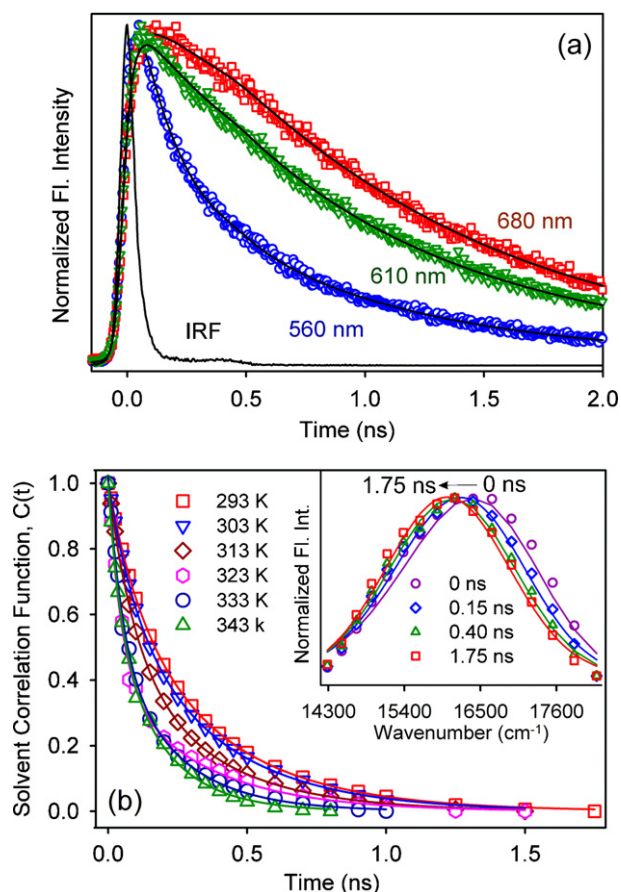


Fig. 2. (a) Fluorescence decays of DCM in 18 mM AOT/water vesicle at 293 K of 560, 610 and 680 nm. (b) Solvent correlation function, $C(t)$ of DCM in 18 mM AOT/water vesicle at 293, 303, 313, 323, 333 and 343 K. The solid lines denote the best fit to biexponential decay. Time-resolved emission spectra of DCM in 18 mM AOT/water vesicle at 293 K are shown in the inset.

rise component of 210 ps is obtained along with decay components of 995 ps and 1800 ps. The presence of faster decay components at the blue end and a rise component at the red wavelength are indicative of solvation in the vesicles. As the temperature is increased to 343 K, the transients still show wavelength dependency, however, with a decrease in the time constants (figures not shown), indicating increased mobility of the solvating species at elevated temperatures.

The time-resolved emission spectra (TRES) of DCM in AOT are constructed at different temperatures following the procedure given in the previous section. A typical TRES for DCM in AOT vesicle as obtained at 293 K is depicted in the inset of Fig. 2b. The $C(t)$ curves obtained at different temperatures are fitted biexponentially (Fig. 2b) and the fitted parameters are presented in Table 1. It is observed from Table 1 that the time constants are in the order of several tens of and several hundreds of picoseconds, respectively. It can be noted that both these components are slower than the subpicosecond solvation time scale reported for bulk water [50]. As has been inferred from steady-state measurements the observed solvation dynamics appear to be due exclusively to the DCM molecules residing at the AOT water interface, a conclusion also supported from the fact that DCM in hydrocarbon produces very short lifetime of ~ 50 ps as opposed to the considerably slow decay time constants found in the present study. The observed average solvation time ($\langle \tau_s \rangle = a_1 \tau_1 + a_2 \tau_2$) of 0.29 ns at 293 K is comparable to that of DCM obtained in the interfacial stern layer of SDS micelle [33]. The two slow time components obtained in the present study have their origin from the relaxation of the

interfacial bound type (hydrogen bonded to the polar headgroup, τ_2) and free type water molecules (not directly hydrogen bonded to the headgroup, but hydrogen bonded to the interfacial-bound water, τ_1) present in the interface of AOT vesicles. This observation also provides supports towards the unilamellarity of AOT vesicles as explained below. The entrapped water pool of unilamellar AOT vesicle is considerably bigger (radius ~ 68.0 nm) than those of the water pool of the reverse micelles (radius < 10 nm). Earlier Bhattacharya et al. reported that in AOT microemulsion ($[H_2O]/[AOT] = 20$), DCM exhibits bimodal solvation dynamics with time components of 0.3 ns and 2.4 ns respectively having an average time constant of 1.23 ns [34]. This solvation time gets faster as the water pool radius increases, which in turn is due to the addition of fast moving bulk water into the system [51]. The present study rather exhibits a faster relaxation time scale compared to that in w/o microemulsion systems. Earlier studies by Xie et al. [28] reveal that MLVs consist of concentric bilayers (onion like structure) with highly structured water molecules present in between the bilayers and thus are expected to exhibit a relatively slow solvation response as also obtained in microemulsion systems [34]. The absence of any such slow relaxation component in the present study thus reconfirms the formation of ULV only as has been proposed from the DLS measurements.

To further investigate possible heterogeneity in the positional distribution of DCM at the vesicle interface we follow time-resolved area normalized emission spectral (TRANES), which is a well-established technique [52–54] and is a modified version of TRES. The unique feature of this method is that existence of an isoemissive point in the spectra indicates the presence of two emitting species in the system (i.e., heterogeneity in the residence of the fluorophore). In the present study, we do not find any isoemissive point when we construct TRANES at any of the studied temperatures (Figure S1 in the supporting information). This observation reconfirms the formation of ULV at the studied AOT concentrations.

Having characterized the uniform size and unilamellarity of the AOT vesicle along with its stability over a range of temperature, it now becomes interesting to study the energetic associated with the dynamical water exchange at the vesicle interface. In this regard, we study the solvation dynamics of AOT vesicle at different temperatures (Fig. 2b) and the fitted solvation data are presented in Table 1. It can be observed from the figure and the table that solvation becomes faster at elevated temperatures, which can be explained with the help of the multishell continuum model proposed by Bagchi et al. for reverse micelles and proteins [55–57]. In this model, a dynamic exchange between bound and free water molecules at the interface is assumed. The energetic of the exchange depends upon the strength and the number of hydrogen bonds among the water molecules at the interface. This bound to free type transition of water molecules with temperature has been shown to follow an Arrhenius type of activation energy barrier crossing model [55,58]. We plot $\ln(1/\langle \tau_s \rangle)$ as a function of $1/T$, and a good linear fit is obtained (Fig. 3a). From the slope of the straight line, activation

Table 1

Solvation correlation data for DCM in 18 mM AOT/water vesicle at different temperatures.^a

Temperature (K)	a_1	τ_1 (ns)	a_2	τ_2 (ns)	$\langle \tau_s \rangle$ (ns)	E_a (kcal mol ⁻¹)
293	0.32	0.11	0.68	0.37	0.29	3.7 ± 0.2
303	0.35	0.10	0.65	0.36	0.26	
313	0.49	0.09	0.51	0.33	0.21	
323	0.60	0.05	0.40	0.32	0.16	
333	0.49	0.05	0.51	0.22	0.14	
343	0.41	0.04	0.59	0.18	0.12	

^a τ_i represents the solvent correlation time constant, a_i represents its relative contribution and $\langle \tau_s \rangle$ the average solvation time constant. Estimated maximum error in determination of τ_i is 6%.

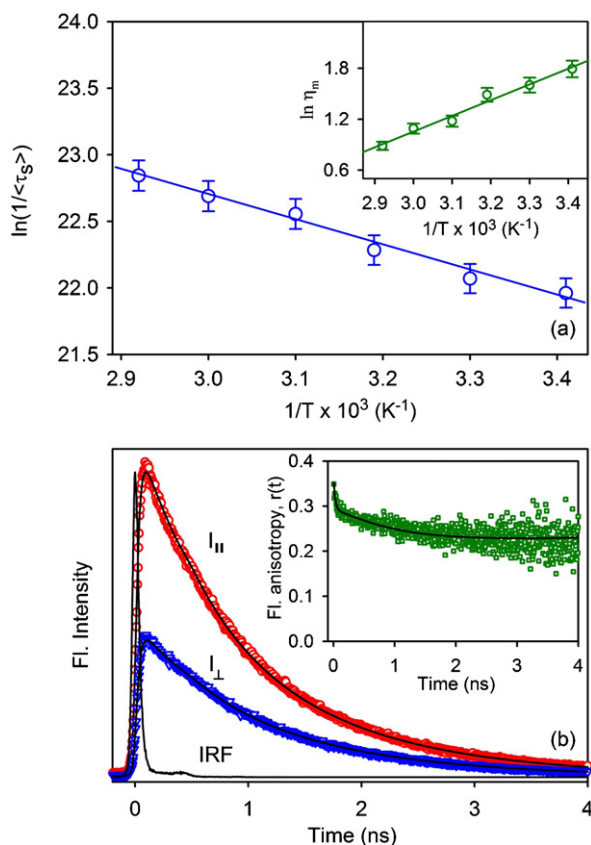


Fig. 3. (a) Plot of $\ln(1/\langle\tau_s\rangle)$, τ_s expressed in second, against $1/T$ for 18 mM AOT/water vesicle, with linear fit. A plot of $\ln(\eta_m)$, η_m expressed in cP, against $1/T$ for the same system is shown in the inset with linear fit. (b) Triexponential reconvolution analyses of $I_{||}(t)$ and $I_{\perp}(t)$ polarized decays of DCM in AOT/water vesicle at 293 K. The temporal anisotropy decay curve (square) generated using Eq. (3), is plotted in the inset and the solid line denotes its best fit.

energy (E_a) is calculated to be 3.7 ± 0.2 kcal mol $^{-1}$, which is of the same order of magnitude to that obtained for the transition from bound type water (hydrogen bonded to polar headgroup) to free type water (not directly hydrogen bonded to headgroup) at RM [59] and micellar [33,60] interface. This equality is a direct consequence of the dynamic nature of the primary and secondary hydration shell near the cell mimicking AOT vesicle which in turn is largely influenced by temperature.

To have a further idea of the temperature-mediated modification of interfacial water dynamics, we measure the temporal anisotropy decay, $r(t)$, of the probe in AOT vesicle at different temperatures. The inset of Fig. 3b shows a representative anisotropy decay of DCM in AOT/water vesicles at 293 K. The time components obtained from fluorescence anisotropy decay, $r(t)$, of DCM in AOT vesicles at different temperatures are listed in Table 2. The time components obtained in this study are significantly slower than the picosecond time scale reported for conventional hydrophobic dyes in bulk water [45] indicating hindered rotation of the probe.

Table 2
Fluorescence anisotropy decays and wobbling-in-cone data of DCM in 18 mM AOT/water vesicle at different temperatures.^a

Temperature (K)	τ_0	a_{fast}	τ_{fast} (ns)	a_{slow}	τ_{slow} (ns)	D_w ($\times 10^{-8}$ s $^{-1}$)	η_m (cP) Simple SED	η_m (cP) Modified SED	E_a (kcal mol $^{-1}$)
293	0.34	0.26	0.55	0.08	2.18	03.19	7.79	5.99	3.6 ± 0.2
303	0.34	0.27	0.44	0.07	1.88	04.15	6.45	4.96	
313	0.33	0.33	0.38	–	–	06.57	5.76	4.42	
323	0.33	0.33	0.27	–	–	09.25	4.22	3.24	
333	0.32	0.32	0.24	–	–	10.41	3.87	2.97	
343	0.33	0.33	0.19	–	–	13.15	3.15	2.42	

^a τ_i represents the anisotropy time constant and a_i represents its relative weight in the total anisotropy. Estimated maximum error in determination of τ_i is 5%.

This concludes that the dye experiences much higher viscosity (see later) in AOT vesicles in comparison to that in bulk water, which concludes the residence of the probe in the interfacial layer of the vesicles at all the studied temperatures. Note that the anisotropy decays at low temperatures are biexponential having a major contribution from the fast component (τ_{fast}). At higher temperatures the contribution of the slower component (τ_{slow}) vanishes making the decay transient single-exponential. To account for the effect of temperature on the rotational relaxation process of the probe in the vesicle, the anisotropy decay is analyzed using the two-step wobbling-in-cone model described elsewhere [61–64]. The diffusion coefficient (D_w) values obtained using this model (Table 2) are of the same order of magnitude as reported earlier for micelle [65] and RM systems [59] and increases with temperature. This increase implies that with increasing temperature, the probe experiences less restricted rotation at the vesicle interface which might originate from the faster movement of the trapped water at elevated temperatures. This change is also manifested in the observed faster solvation dynamics at elevated temperatures (Table 1 and Fig. 2b). The interfacial microviscosity η_m as experienced by the probe can be estimated from the time-resolved fluorescence anisotropy using the modified Stokes–Einstein–Debye equation (SED) [66,67],

$$\tau_r = \frac{\eta_m V_h}{k_B T} \quad (12)$$

where k_B is the Boltzmann constant, T the absolute temperature. Hydrodynamic volume of the probe (V_h) can be calculated as:

$$V_h = V_m f C \quad (13)$$

where f is the shape factor ($f=1$ for a spherical probe) and C represents solute–solvent coupling constant ($C=1$ for “stick” condition and $C < 1$ for “slip” condition) and V_m the molecular volume of the probe [68]. In case of $f=C=1$, Eq. (12) reduces to the original simple SED equation,

$$\tau_r = \frac{\eta_m V_m}{k_B T} \quad (14)$$

While estimating microviscosities we have used the simple SED (Eq. (14)) as well as the modified SED (Eqs. (12) and (13)) model considering realistic f and C values. Fixing DCM as a prolate ellipsoid [69] with a molecular volume of ~ 285 Å 3 (estimated according to the procedure described elsewhere [70]), the value of f is calculated using the equation [66,67],

$$f = \frac{2}{3} \frac{1 - p^4}{[(2 - p^2)p^2(1 - p^2)^{-1/2} \ln((1 + (1 - p^2)^{1/2})/p)] - p^2} \quad (15)$$

where p is the axial ratio (ratio of minor axis to major axis) of the prolate ellipsoid. For DCM, the shape factor, f , is estimated to be 2.56. As the coupling constant C also depends on the boundary condition (slip or stick), we have estimated the microviscosities by considering the coupling factor to be 0.508 for slipping boundary condition as calculated for a nonspherical probe [68]. The estimated microviscosity values calculated by both simple SED and modified SED are presented in Table 2. It is evident from the table that the values of microviscosity are ~ 6 times higher than that of bulk water.

Table 3

Calculated values of parameters obtained from FRET between H258 & EtBr and H258 & DCM pairs at 293 K.^a

System	$\langle\tau_D\rangle$ (ns)	$\langle\tau_{DA}\rangle$ (ns)	$J(\lambda)$ (M ⁻¹ cm ⁻¹ nm ⁴)	E	R_0 (nm)	R (nm)
H258-EtBr	2.18	0.66	2.50×10^{14}	0.70 ± 0.003	3.4	3.0 ± 0.04
H258-DCM	2.25	1.09	15.2×10^{14}	0.52 ± 0.004	4.7	4.6 ± 0.05

^a $\langle\tau_D\rangle$ and $\langle\tau_{DA}\rangle$ represents the average fluorescence lifetime of the donor in absence and presence of the acceptor, respectively. Estimated error in determination of τ_D and τ_{DA} is 3%.

Earlier reports suggest that microviscosity in micelle [65] and RM [71] system are 10–15 and 6–9 times higher than that in bulk water, respectively. It is also observed that η_m decreases gradually with increasing temperature revealing that the probe experiences less rotational hindrance at higher temperature which might results from the breaking of water–water hydrogen bond network at the interface. Assuming that microviscosity changes with temperature following the relation [72],

$$\eta_m = \eta_0 \exp\left(\frac{E_\eta}{RT}\right) \quad (16)$$

where E_η is the energy barrier for the viscous flow. Using the η_m values obtained from Eq. (12) we plot $\ln \eta_m$ against $1/T$ (inset of Fig. 3a) and a good linear fit is obtained with a calculated E_η value of 3.6 ± 0.2 kcal mol⁻¹. The good agreement between the E_η obtained from the rotational anisotropy study and E_a value obtained from solvation dynamics study is notable. The close agreement between these two energy values indicate the cooperatively of the two processes involved. As discussed earlier, the observed acceleration of the solvation dynamics with temperature has its origin in the transition of the slower moving interfacially bound water to faster moving bulk-type water, which in turn is associated with the decrease in the microviscosity at the vesicle interface.

To investigate the ability of AOT vesicles to host drugs of various nature (both hydrophobic and charged) simultaneously we study FRET between the dyes H258 (donor) and DCM (acceptor), and also between H258 (donor) and EtBr (acceptor) in AOT vesicles after solubilising each donor acceptor pair in AOT vesicles. Fig. 4 shows that an efficient energy transfer takes place between each donor–acceptor pair, as indicated by the faster decay of the donor in presence of the acceptor in the vesicles compared to that of the donor itself in the vesicles. The estimated donor–acceptor distances between H258 and DCM pair and H258 and EtBr pair are calculated to be 4.6 ± 0.05 and 3.0 ± 0.04 nm respectively using Eq. (10) (Table 3). The observed FRET distances are much smaller than the estimated inter vesicle distance of ~ 120 nm supporting energy transfer between the donor–acceptor pairs hosted simultaneously in the same AOT vesicle. The finding shows the ability of the AOT vesicles to host simultaneously both charged drugs like H258, EtBr and also hydrophobic model drug DCM. This is very crucial for many codelivery applications and supports the strong candidature of AOT vesicles among drug nano carriers.

An interesting question at this juncture is whether the AOT vesicles produced could evolve as a convenient drug carrier. A good drug nano carrier should prerequisite be able to release a drug in a controlled manner. To investigate the release profile of AOT vesicle a well known anti-tuberculosis drug rifampicin [73] is taken as a model. Plot of cumulative percent of drug released against time (Fig. 5a) shows a typical profile of first order exponential controlled release of the drug [74,75]. The release profile follows a relation,

$$Q = Q_0 - be^{-Kt} \quad (17)$$

where Q is the cumulative percent of drug released at time t , b a constant and K the rate constant of drug release. At pH 7.4, 60% of the drug is released from the vesicles in 6.5 h whereas 80% of it is released within the first 6.0 h in a controlled experiment without AOT vesicle (Fig. 5a). This clearly indicates that AOT vesicle

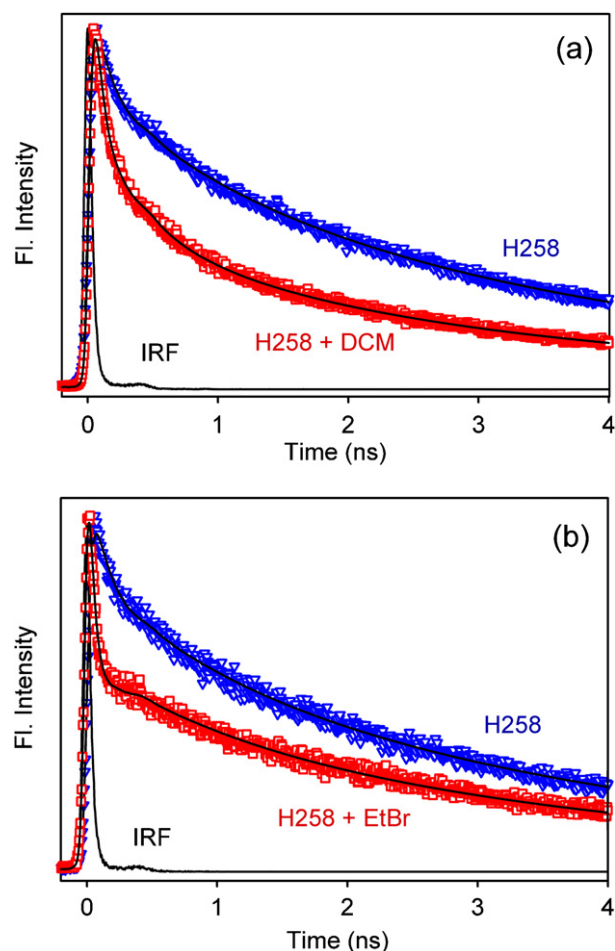


Fig. 4. (a) The temporal decay of H258 and H258-DCM FRET pair in 18 mM AOT/water vesicles monitored at 490 nm. (b) The temporal decay of H258 and H258-EtBr FRET pair in 18 mM AOT/water vesicles monitored at 490 nm.

helps in increasing the dosage time making the drug available for a longer period of time without degradation. The release of rifampicin loaded vesicles is studied further in an acidic pH of 5.8 as rifampicin shows variation in solubility with pH [76] which in turn could affect its bioavailability. As observed from Fig. 5a an acidic environment not only retards the rate of release but also the extent of rifampicin release. The decrease of drug release at lower pH is also evident from the K value obtained by fitting the curves with Eq. (17) (Fig. 5a and Table 4). Decreasing pH from 7.4 to 5.8 is manifested in a 3 fold decreases in the rate of rifampicin release from AOT vesicle whereas

Table 4

Rate constant values using first order exponential equation for the release of rifampicin from AOT vesicles and water.

pH	K (h ⁻¹)		n
	Control	AOT vesicle	AOT vesicle
7.4	0.45 ± 0.01	0.24 ± 0.01	0.79 ± 0.03
5.8	0.40 ± 0.02	0.08 ± 0.01	0.65 ± 0.01

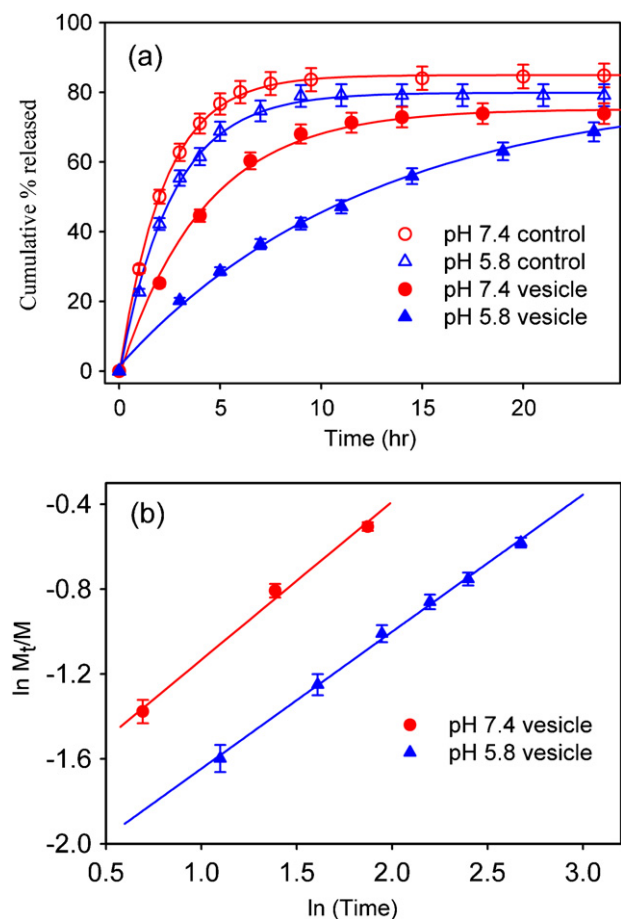


Fig. 5. (a) Release profile of rifampicin from AOT vesicle at pH 7.4, 5.8. The solid lines are fits according to Eq. (17). (b) Peppas fit (Eq. (18)) at pH 7.4 and 5.8 with time expressed in hours.

the change is negligible in the control experiment. It is reported that at various pH medium the dissolution rate depends on the interaction of rifampicin with the acidic excipients like SDS and AOT [77]. In our case also the observed retardation might originate from the interaction of rifampicin with AOT, which in turn could modulate rifampicin bioavailability.

The mechanism of drug release can be analyzed by a relationship proposed by Peppas et al. [78]:

$$\frac{M_t}{M} = kt^n \quad (18)$$

where M_t/M is the fraction of drug released at time t , k a kinetic constant relative to the properties of the matrix and the drug (structural and geometric characteristics) and n the diffusional exponent, which depends upon the release mechanism and geometry of the device. It has been shown that this relation can adequately describe the release of drugs or other solutes from slabs, cylinders and spheres, regardless of the release mechanism [78]. The value of k and n can be calculated from the intercept and slope of the straight line plotted for the first 60% of the release curves. We obtain good linear fits (Fig. 5b) with corresponding n values of 0.79 ± 0.03 at pH 7.4 and 0.65 ± 0.01 at pH 5.8. It should be noted here that for spherical carrier n should be equal to 0.5 for a pure Fickian release, 1 for zero-order kinetics and $0.5 < n < 1$ for anomalous (non-Fickian) release [78]. In the present system the release of rifampicin from AOT vesicle is found to be non-Fickian in nature.

4. Conclusion

We have explored the aggregate structure and size of AOT vesicles in dilute aqueous region (9–18 mM AOT), using the combination of spectroscopic and light scattering methods. The size of the AOT vesicles (monodispersed in distribution) is found to be independent of temperature (293–343 K) and surfactant concentration (9, 14 and 18 mM) providing evidence of its unilamellarity. The time independent DLS data further shows its aging stability. Microenvironment of the AOT vesicles is probed through a solvation probe, DCM. Both steady-state and time-resolved fluorescence spectroscopy indicate the residence of the probe DCM at the surfactant water interface and shows the efficacy of the vesicles to host the model drug/ligand DCM. A comparably faster solvation dynamics ($\langle \tau_s \rangle = 0.29$ ns) in AOT vesicle compared to AOT microemulsion ($\langle \tau_s \rangle = 1.23$ ns) rules out the presence of multiple concentric bilayers as has also been evidenced from the DLS study. Absence of an isoemissive point in TRANES further rules out the heterogeneity in the residence of DCM molecules. The residence of the probe in the solvation shell of the AOT vesicle has been confirmed through the increased microviscosity of the probe environment, compared to the bulk viscosity of the solution. The time resolved FRET studies between various dyes present in the same vesicles show the ability of the AOT vesicles to host model drugs of various natures simultaneously. The drug release from the vesicle is found to be controlled over 24 h at 37 °C at both the studied pH range of the dissolution medium. The release rate changes in acidic pH. All these features hold great promise for the development of AOT vesicles as viable drug delivery systems. The study explores the hydrogen bonded structure and dynamics at the interface of the AOT vesicle, which is similar to the environment around cell. The considerable stability of the nontoxic, monodispersed, unilamellar AOT/water vesicles in wide range of AOT concentration and temperature, with the capability of hosting drugs of various natures simultaneously for many codelivery applications combined with controlled drug release profile may find its application in drug delivery.

Acknowledgement

P.K.V. thanks CSIR for fellowship. We thank DST for the financial support (SR/SO/BB-15/2007).

Appendix A. Supplementary data

Supplementary data associated with this article can be found, in the online version, at doi:10.1016/j.colsurfb.2011.07.012.

References

- [1] J.H. Fendler, Chem. Mater. 8 (1996) 1616.
- [2] G. Gregoriadis, Liposome Technology, CRC Press, FL, 1984.
- [3] H.C. Youn, B. Subhash, J.H. Fendler, J. Phys. Chem. 92 (1988) 6320.
- [4] D.D. Lasic, Liposomes: From physics to Application, Elsevier, New York, 1993.
- [5] T.M. Allen, C. Hansen, F. Martin, C. Redemann, A.Y. Young, Biochim. Biophys. Acta 1066 (1991) 29.
- [6] C. Guo, S. Liu, Z. Dai, C. Jiang, W. Li, Colloids Surf. B 76 (2010) 362.
- [7] O.V. Gerasimov, J.A. Boomer, M.M. Qualls, D.H. Thompson, Adv. Drug Delivery Rev. 38 (1999) 317.
- [8] R.S. Langer, D.L. Wise (Eds.), Medical Applications of Controlled Release, Applications and Evaluation, vols. I and II, CRC Press, Boca Raton, Florida, 1984.
- [9] M. Grassi, University of Trieste, VIII ciclo, 1996.
- [10] J.R. Robinson, V.H.L. Lee (Eds.), Controlled Drug Delivery, Marcel Dekker, Inc., New York, Basel, 1987.
- [11] A.M. Carmona-Ribeiro, L.S. Yoshida, A. Sesso, H. Chaimovich, J. Colloid Interface Sci. 100 (1984) 433.
- [12] J.E. Brady, D.F. Evans, B. Kachar, B.W. Ninham, J. Am. Chem. Soc. 106 (1984) 4279.
- [13] Y. Talmon, D.F. Evans, B.W. Ninham, Science 221 (1983) 1047.
- [14] N.E. Gabriel, M.F. Roberts, Biochemistry 23 (1984) 4011.
- [15] H. Fukuda, K. Kawata, H. Okuda, S.L. Regen, J. Am. Chem. Soc. 112 (1990) 1635.
- [16] Z. Lin, M. He, L.E. Scriven, H.T. Davis, J. Phys. Chem. 97 (1993) 3571.

- [17] J. Hao, H. Hoffmann, K. Horbaschek, *Langmuir* 17 (2001) 4151.
- [18] M. Mao, J. Huang, B. Zhu, H. Yin, H. Fu, *Langmuir* 18 (2002) 3380.
- [19] H.T. Jung, B. Coldren, J.A. Zasadzinski, D.J. Iampietro, E.W. Kaler, *Proc. Natl. Acad. Sci. U.S.A.* 98 (2001) 1353.
- [20] E.F. Marques, *Langmuir* 16 (2000) 4798.
- [21] A.J. O'Connor, T.A. Hatton, A. Bose, *Langmuir* 13 (1997) 6931.
- [22] C. Cailliet, M. Hebrant, C. Tondre, *Langmuir* 16 (2000) 9099.
- [23] K.L. Herrington, E.W. Kaler, D.D. Miller, J.A. Zasadzinski, S. Chiruvolu, *J. Phys. Chem.* 97 (1993) 13792.
- [24] D.J. Iampietro, L.L. Brasher, E.W. Kaler, A. Stradner, O. Glatter, *J. Phys. Chem. B* 102 (1998) 3105.
- [25] T.K. De, A. Maitra, *Adv. Colloid Interface Sci.* 59 (1995) 95.
- [26] S.N. Malik, D.H. Canaham, M.W. Gouda, *J. Pharm. Sci.* 64 (1975) 987.
- [27] M. Varshney, T. Khanna, M. Changez, *Colloids Surf. B* 13 (1999) 1.
- [28] J.-X. Cheng, S. Pautot, D.A. Weitz, X.S. Xie, *Proc. Natl. Acad. Sci. U.S.A.* 100 (2003) 9826.
- [29] J. Rogers, P.A. Winsor, *Nature* 216 (1967) 477.
- [30] J.I. Briz, M.M. Velázquez, *J. Colloid Interface Sci.* 247 (2002) 437.
- [31] G.H. Sagar, J.R. Bellare, *J. Phys. Chem. B* 113 (2009) 13805.
- [32] T.A. Horbett, B.D. Ratner, J. Kost, M. Singh, in: J.M. Anderson, S.W. Kim (Eds.), *Recent Advances in Drug Delivery Systems*, Plenum Press, New York, 1984, p. 209.
- [33] R.K. Mitra, S.S. Sinha, S.K. Pal, *J. Phys. Chem. B* 111 (2007) 7577.
- [34] S.K. Pal, D. Mandal, D. Sukul, K. Bhattacharyya, *Chem. Phys. Lett.* 312 (1999) 178.
- [35] S.K. Pal, D. Sukul, D. Mandal, K. Bhattacharyya, *J. Phys. Chem. B* 104 (2000) 4529.
- [36] J.R. Lakowicz, *Principles of Fluorescence Spectroscopy*, Kluwer Academic/Plenum, New York, 1999.
- [37] P. Kapusta, R. Erdmann, U. Ortmann, M. Wahl, *J. Fluoresc.* 13 (2003) 179.
- [38] H. Gorner, *Photochem. Photobiol.* 73 (2001) 339.
- [39] J.A. Omotosho, T.L. Whateley, A.T. Florence, *J. Microencapsul.* 6 (1989) 183.
- [40] Y. Fan, Y. Li, G. Yuan, Y. Wang, J. Wang, C.C. Han, H. Yan, *Langmuir* 21 (2005) 3814.
- [41] I.M. Umlong, K. Ismail, *J. Colloid Interface Sci.* 291 (2005) 529.
- [42] C. Lin, J. Zhao, R. Jiang, *Chem. Phys. Lett.* 464 (2008) 77.
- [43] A. Chatterjee, S.P. Moulik, S.K. Sanyal, B.K. Mishra, P.M. Puri, *J. Phys. Chem. B* 105 (2001) 12823.
- [44] T.M. Bayerl, M. Bloom, *Biophys. J.* 58 (1990) 357.
- [45] D. Banerjee, P.K. Verma, S.K. Pal, *Photochem. Photobiol. Sci.* 8 (2009) 1441.
- [46] S.K. Pal, D. Sukul, D. Mandal, S. Sen, K. Bhattacharyya, *Chem. Phys. Lett.* 327 (2000) 91.
- [47] M. Meyer, J.C. Mialocq, *Opt. Commun* 64 (1987) 264.
- [48] Z. Hsing-Kang, M. Ren-Lan, N. Er-pin, G. Chu, *J. Photochem.* 29 (1985) 397.
- [49] D.C. Easter, A.P. Baronavski, *Chem. Phys. Lett.* 201 (1993) 153.
- [50] R. Jimenez, G.R. Fleming, P.V. Kumar, M. Maroncelli, *Nature* 369 (1994) 471.
- [51] P.K. Verma, A. Makhil, R.K. Mitra, S.K. Pal, *Phys. Chem. Chem. Phys.* 11 (2009) 8467.
- [52] N. Periasamy, A.S.R. Koti, *Proc. Indian Natn. Sci. Acad.* 69A (2003) 41.
- [53] A.S.R. Koti, N. Periasamy, *Proc. Indian Acad. Sci. (Chem. Sci.)* 113 (2001) 157.
- [54] A.S.R. Koti, M.M.G. Krishna, N. Periasamy, *J. Phys. Chem. A* 105 (2001) 1767.
- [55] N. Nandi, B. Bagchi, *J. Phys. Chem. B* 101 (1997) 10954.
- [56] N. Nandi, K. Bhattacharyya, B. Bagchi, *Chem. Rev.* 100 (2000) 2013.
- [57] N. Nandi, B. Bagchi, *J. Phys. Chem. A* 102 (1998) 8217.
- [58] R.K. Mitra, P.K. Verma, D. Banerjee, S.K. Pal, in: K.-L. Han, G.-J. Zhao (Eds.), *Hydrogen Bonding and Transfer in the Excited State*, vol. 1, John Wiley, Chippenharn, 2010, p. 217.
- [59] R.K. Mitra, S.S. Sinha, S.K. Pal, *Langmuir* 24 (2008) 49.
- [60] S. Pal, S. Balasubramanian, B. Bagchi, *J. Phys. Chem. B* 107 (2003) 5194.
- [61] G. Lipari, A. Szabo, *J. Chem. Phys.* 75 (1981) 2971.
- [62] G. Lipari, A. Szabo, *J. Am. Chem. Soc.* 104 (1982) 4546.
- [63] G. Lipari, A. Szabo, *Biophys. J.* 30 (1980) 489.
- [64] C.C. Wang, R. Pecora, *J. Chem. Phys.* 72 (1980) 5333.
- [65] G.B. Dutt, *J. Phys. Chem. B* 108 (2004) 3651.
- [66] L.A. Philips, S.P. Webb, J.H. Clark, *J. Chem. Phys.* 83 (1985) 5810.
- [67] B. Kalman, N. Clarke, L.B.A. Johansson, *J. Phys. Chem.* 93 (1989) 4608.
- [68] N. Ito, O. Kajimoto, K. Hara, *Chem. Phys. Lett.* 318 (2000) 118.
- [69] P.M. Wallace, D.R.B. Sluss, L.R. Dalton, B.H. Robinson, P.J. Reid, *J. Phys. Chem. B* 110 (2006) 75.
- [70] Y.H. Zhao, M.H. Abraham, A.M. Zissimos, *J. Org. Chem.* 68 (2003) 7368.
- [71] E.M. Corbeil, R.E. Riter, N.E. Levinger, *J. Phys. Chem. B* 108 (2004) 10777.
- [72] R. Zana, *J. Phys. Chem. B* 103 (1999) 9117.
- [73] J.W. Long, *Essential Guide to Prescription Drugs 1992*, HarperCollins Publishers, New York, 1991.
- [74] H. Dai, Q. Chen, H. Qin, Y. Guan, D. Shen, Y. Hua, Y. Tang, J. Xu, *Macromolecules* 39 (2006) 6584.
- [75] L. Zhang, X. Sun, Z.-R. Zhang, *Drug Delivery* 12 (2005) 289.
- [76] T.T. Mariappan, S. Singh, *Int. J. Tuberc. Lung Dis.* 7 (2003) 797.
- [77] S. Agrawal, R. Panchagnula, *Int. J. Pharm.* 287 (2004) 97.
- [78] P.L. Ritger, N.A. Peppas, *J. Controlled Release* 5 (1987) 23.